Nonlinear Analysis: Modelling and Control, Vol. 31, No. 6, 1280–1303
https://doi.org/10.15388/namc.2026.31.49068

Vilnius University Press

Stability and vegetation patterns driven by both nonlocal infiltration and nonlocal absorption in the extended Klausmeier model*

Yunzhuo Lin, Yongli Song, Shuyang Xue

School of Mathematics, Hangzhou Normal University,
Hangzhou 311121, China
songyl@hznu.edu.cn; 20223057@hznu.edu.cn

Received: March 3, 2026 / **Revised:** July 20, 2026 / **Published online:** October 15, 2026

Abstract. In this paper, we propose a dryland ecosystem model with both nonlocal infiltration and nonlocal absorption and investigate the influence of the nonlocal effect on the vegetation patterns. For the local model, the existence and stability of the nonnegative equilibria are theoretically investigated. For the diffusive model without nonlocal effect, diffusion-driven Turing instability and the critical value of the diffusion coefficient are determined. For the diffusive model with nonlocal effects characterized by the spatial average kernel, the mode-1 steady state bifurcation occurs. For the diffusive model with nonlocal effects characterized by the top-hat kernel, it has been shown that a transition of vegetation patterns occurs when the scale of nonlocal infiltration and nonlocal absorption varies.

Keywords: dryland ecosystem model, stability, bifurcation, patterns.

1 Introduction

In arid and semiarid regions, the imbalance between vegetation dynamics and water availability is a major driver of land degradation and desertification, posing significant threats to ecological sustainability, human livelihoods, and long-term socioeconomic development [7, 10]. Maintaining sufficient vegetation cover is recognized as an effective strategy for mitigating desertification, while precipitation serves as a primary limiting factor for vegetation growth and recovery. Therefore, understanding the complex interactions between vegetation and water is essential not only for elucidating the mechanisms underlying vegetation pattern formation but also for guiding ecosystem management and developing strategies to enhance resilience against desertification under changing climatic conditions [2, 11]. Field observations have shown that vegetation patterns can be broadly categorized into several types, including spot patterns, stripe patterns, labyrinthine patterns, fairy circle patterns, and banded patterns [15, 20].

*This research was supported by the National Natural Science Foundation of China (Nos. 12371166 and 12401637).

© 2026 The Author(s). Published by Vilnius University Press
This is an Open Access article distributed under the terms of the Creative Commons Attribution Licence, which permits unrestricted use, distribution, and reproduction in any medium, provided the original author and source are credited.

Over the past several decades, an increasing number of scholars have incorporated diverse factors into vegetation–water models to explore the mechanisms underlying vegetation pattern formation, thereby advancing our understanding of their dynamical processes. Factors such as root distribution, water infiltration capacity, slope gradient, and soil texture have been demonstrated to play critical roles in the emergence and evolution of vegetation patterns. In 1999, Klausmeier first proposed the following famous dryland ecosystem model for the slope environment in [6]:

$$\begin{aligned} \frac{\partial W}{\partial T} &= V\frac{\partial W}{\partial X} + Q - EW - RG(W)F(P)P, \\ \frac{\partial P}{\partial T} &= D\Delta P + JRG(W)F(P)P - \eta P, \end{aligned} \tag{1}$$

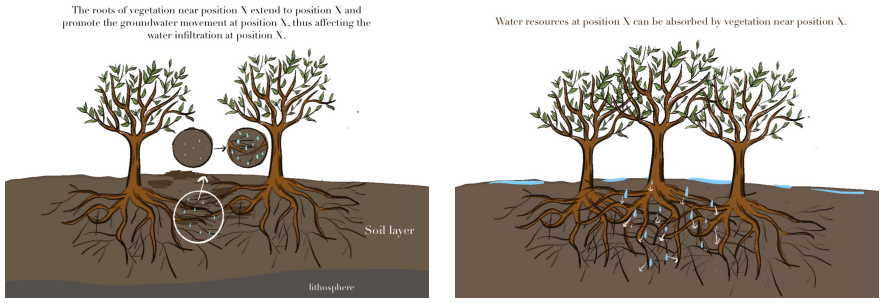
where W and P represent water and vegetation biomass, respectively, $G(W)$ represents the water consumption per unit plant, $F(P)$ represents the influence of plants on water infiltration. For more biological explanations of the model, refer to [6]. After Klausmeier's pioneering work, the study on the pattern formation in dryland ecosystems has attracted attention from scholars in the fields of ecosystems and biomathematics, and a plenty of modified Klausmeier models have been introduced for different semiarid environments [5, 13, 14].

In particular, considering the density-dependent growth rate of the vegetation and a flat environment, Bastiaansen et al. [1] proposed the following modified Klausmeier model:

$$\begin{aligned} \frac{\partial W}{\partial T} &= D_1\Delta W + Q - EW - RWP^2, \\ \frac{\partial P}{\partial T} &= D_2\Delta P + RJ\left(1 - \frac{P}{C}\right)WP^2 - \eta P, \end{aligned} \tag{2}$$

where C is the carrying capacity. Compared with model (1), the term $1 - P/C$ implies that the conversion rate of the plant biomass decreases as P increases for $P < C$.

However, nonlocal interactions may represent a crucial mechanism underlying the formation of vegetation patterns [12]. In the previous work, vegetation at location X enhances water permeability by loosening the soil, reflecting local permeability since the infiltration capacity is solely dependent on the amount of vegetation at location X. The study in [6] hypothesized a proportional relationship between infiltration capacity and the vegetation cover at location X. However, considering that vegetation surrounding location X can also influence the water permeability at this location by extending its root systems to loosen the soil at location X, this represents a nonlocal effect on permeability, since the infiltration capacity of water in the case is not only determined by the vegetation cover at location X but is also influenced by the vegetation density in the surrounding area, as illustrated in Fig. 1(a). In addition, during water uptake by the root systems, vegetation absorbs water not only from its current surroundings but also from the vicinity of neighboring root systems, as shown in Fig. 1(b).



(a) (b)

Figure 1. (a) Nonlocal infiltration; (b) nonlocal absorption.

Motivated by these ideas, we introduce nonlocal infiltration and nonlocal absorption into (2) and consider the following model:

$$\begin{aligned}
\frac{\partial W}{\partial T} &= D_1 \frac{\partial^2 W}{\partial X^2} + Q - EW \\
&\quad - RW \underbrace{\int_\Omega \Phi\big(|X-Y|\big)P(Y,T)\,\mathrm{d}Y}_{\text{nonlocal infiltration}} \underbrace{\int_\Omega \Phi\big(|X-Y|\big)P(Y,T)\,\mathrm{d}Y}_{\text{nonlocal absorption}}, \\
\frac{\partial P}{\partial T} &= D_2 \frac{\partial^2 P}{\partial X^2} + RJP^2\left(1-\frac{P}{C}\right) \underbrace{\int_\Omega \Phi\big(|X-Y|\big)W(Y,T)\,\mathrm{d}Y}_{\text{nonlocal absorption}} - \eta P.
\end{aligned} \tag{3}$$

For the W-equation, it is assumed that there exists a region Ω centered at X such that Ω represents the root range of plants, and all the plants $P(Y,T)$ within Ω absorb the water at position X. Root growth enhances soil permeability, thereby accelerating water depletion, and the spatial extent of this process is governed by root distribution. Since both infiltration (mediated by soil properties) and absorption (mediated by roots) are driven by the same underlying mechanism, namely the spatial footprint of the root system, the nonlocal consumption of water by plants is characterized by the term $RW\int_\Omega \Phi(|X-Y|)\times P(Y,T)\,\mathrm{d}Y\int_\Omega \Phi(|X-Y|)P(Y,T)\,\mathrm{d}Y$, where the weighting function $\Phi(|X-Y|)$ reflects the spatial influence of vegetation at location Y on water dynamics at location X. The weighting function $\Phi(|X-Y|)$ is highly critical in nonlocal models, and different kinds of kernel functions have an important influence on the dynamics [3, 4, 8, 16–18].

In the P-equation, the nonlocal absorption term $\int_\Omega \Phi(|X-Y|)W(Y,T)\,\mathrm{d}Y$ quantifies water uptake by plants at X from surrounding locations, reflecting a resource-dependent growth mechanism. Notice that in the W-equation, the nonlocal absorption term is described by $\int_\Omega \Phi(|X-Y|)P(Y,T)\,\mathrm{d}Y$. This asymmetry embodies a unidirectional resource flow (P consumes W) consistent with established nonlocal vegetation models in [19], where spatial interactions are mediated by biological uptake rather than reciprocal exchange.

To reduce the number of parameters, the following transformation is applied:

$$w=\sqrt{\frac{R}{E}}JW,\qquad p=\sqrt{\frac{R}{E}}P,\qquad t=ET,\qquad a=\frac{JQ}{E}\sqrt{\frac{R}{E}},$$
$$c=\sqrt{\frac{R}{E}}\frac{1}{C},\qquad m=\frac{\eta}{E},\qquad d=\frac{D_1}{D_2},\qquad x=\sqrt{\frac{E}{D_2}}X.$$

Then model (3) becomes the following dimensionless model:

$$\begin{aligned}\frac{\partial w}{\partial t}&=d\frac{\partial^2 w}{\partial x^2}+a-w-w(K*p)^2,\\ \frac{\partial p}{\partial t}&=\frac{\partial^2 p}{\partial x^2}+(K*w)p^2\left(1-\frac{p}{c}\right)-mp\end{aligned}\tag{4}$$

with the nonlocal terms

$$K*p=\int_{\Omega}\phi\big(|x-y|\big)p(y,t)\,\mathrm{d}y,\qquad K*w=\int_{\Omega}\phi\big(|x-y|\big)w(y,t)\,\mathrm{d}y,$$

and $\phi(|x-y|)=\Phi(\sqrt{D_2/E}|X-Y|)$. The main subject of this paper is to investigate the complex spatiotemporal dynamics triggered by the nonlocality for two kinds of nonlocal kernel functions: one is the spatial average kernel function [17], and the other is the top-hat kernel function [16, 18].

The rest of the paper is organized as follows. In Section 2, we consider the existence and stability of the nonnegative equilibria for the local model. In Section 3, we investigate the diffusion-driven Turing instability for the diffusive model without nonlocal terms. In Section 4, we study the spatiotemporal dynamics induced by the nonlocal effects for system (4) for the spatial average kernel and top-hat kernel. Finally, a brief conclusion and discussion in Section 5. Throughout this paper, we denote the set of the positive integers by $\mathbb{N}$ and $\mathbb{N}_0=\{0\}\cup\mathbb{N}$. We write $\mathbb{C}$ for the set of complex numbers and $\mathbb{R}$ for the set of real numbers.

2 Stability and bifurcation analysis for the local model

In this section, we perform the stability and bifurcation analysis for the following ordinary differential equation (ODE) system:

$$\frac{\mathrm{d}w}{\mathrm{d}t}=a-w-wp^2,\qquad \frac{\mathrm{d}p}{\mathrm{d}t}=wp^2\left(1-\frac{p}{c}\right)-mp.\tag{5}$$

Obviously, system (5) always has a boundary equilibrium $E_w(a,0)$, and the positive equilibrium is determined by the following algebraic equation:

$$a-w-wp^2=0,\qquad wp\left(1-\frac{p}{c}\right)-m=0.\tag{6}$$

By a simple calculation, we first have the following results on the existence of the positive equilibria for system (5).

Theorem 1. *For fixed $c, m > 0$, let*

$$a_* = \frac{2m(1+\sqrt{1+c^2})}{c}. \tag{7}$$

Then we have the following results on the existence of positive equilibria:

(i) *when $0 < a < a_*$, system* (5) *has no positive equilibrium*;

(ii) *when $a = a_*$, there is only one positive equilibrium $E_*(w_*, p_*)$, where*

$$w_* = \frac{a_*}{1+p_*^2}, \qquad p_* = \frac{a_* c}{2(mc+a_*)}; \tag{8}$$

(iii) *when $a > a_*$, there exist two positive equilibria $E_-(w_-, p_-)$ and $E_+(w_+, p_+)$, where*

$$w_\pm = \frac{a}{1+p_\pm^2}, \qquad p_\pm = \frac{ac \pm \sqrt{(ac)^2 - 4mc(mc+a)}}{2(mc+a)}. \tag{9}$$

In what follows, we investigate the stability and the possible bifurcation phenomenon of the equilibria. Assume that $\tilde{E} = (\tilde{w}, \tilde{p})$ is the equilibrium of (5). The linearized system of (5) at $\tilde{E}$ is

$$\begin{pmatrix} \frac{\mathrm{d}w}{\mathrm{d}t} \\ \frac{\mathrm{d}p}{\mathrm{d}t} \end{pmatrix} = J \begin{pmatrix} w \\ p \end{pmatrix}, \tag{10}$$

where

$$J = \begin{pmatrix} -1-\tilde{p}^2 & -2\tilde{w}\tilde{p} \\ \tilde{p}^2(1-\frac{\tilde{p}}{c}) & 2\tilde{w}\tilde{p} - \frac{3\tilde{w}\tilde{p}^2}{c} - m \end{pmatrix}. \tag{11}$$

Then the characteristic equation of linear system (10) is

$$\lambda^2 - \mathrm{Tr}(J)\lambda + \mathrm{Det}(J) = 0, \tag{12}$$

where

$$\mathrm{Tr}(J) = -1 - \tilde{p}^2 + 2\tilde{w}\tilde{p} - \frac{3\tilde{w}\tilde{p}^2}{c} - m,$$

$$\mathrm{Det}(J) = (-1-\tilde{p}^2)\left(2\tilde{w}\tilde{p} - \frac{3\tilde{w}\tilde{p}^2}{c} - m\right) + 2\tilde{w}\tilde{p}^3\left(1 - \frac{\tilde{p}}{c}\right).$$

The local stability of the equilibrium depends on the distribution of the characteristic roots, and we have the following theorem on the stability and bifurcation.

Theorem 2. *For system* (5)*, assume that a_* is defined by* (7)*.*

(I) *The boundary equilibrium $E_w = (a, 0)$ is locally asymptotically stable for any $a, c, m > 0$.*

(II) *For the positive equilibria and fixed $c > 0$, we have the following results*:

(i) *when $a > a_*$, the positive equilibrium $E_-(w_-, p_-)$ is unstable, and it is a saddle*;

(ii) *when $a > a_*$, for the positive equilibrium $E_+(w_+, p_+)$, we have*

(a) *if $0 < m \leqslant 2 + 2/c^2$, then $E_+(w_+, p_+)$ is locally asymptotically stable*;

(b) *if* $m > 2 + 2/c^2$*, then there exists a critical value* $a = a_H(m)$ *with* $a_* < a_H(m) < mc + 4m/c$ *such that* $E_+(w_+, p_+)$ *is locally asymptotically stable for* $a > a_H(m)$ *and unstable for* $a_* < a < a_H(m)$*, and system* (5) *undergoes a Hopf bifurcation at* $a = a_H(m)$*. In addition, the function* $a = a_H(m)$*,* $m > 2 + 2/c^2$*, is increasing with respect to* m*.*

(iii) *when* $a = a_*$*, system* (5) *undergoes a saddle-node bifurcation at* $E_*(w_*, p_*)$ *for* $m \neq 2+2/c^2$ *and undergoes a Bogdanov–Takens bifurcation at* $E_*(w_*, p_*)$ *for* $m = 2 + 2/c^2$*.*

Proof. For the boundary equilibrium $E_w = (a, 0)$, we have $\mathrm{Tr}(J) = -1 - m < 0$, $\mathrm{Det}(J) = m > 0$. This implies that the two characteristic roots at E_w both have negative real parts. Therefore, E_w is locally asymptotically stable. The proof of (I) is completed.

For E_* and $E_\pm$ and letting $Q = (ac)^2 - 4mc(mc + a)$, it is easy to see that $Q \geqslant 0$ is equivalent to $a \geqslant a_*$, and $Q = 0$ for E_* and $Q > 0$ for $E_\pm$.

When $a > a_*$, from (6) and (9) we have for E_-,

$$\mathrm{Det}(J)|_{E_-} = w_- p_- \left(p_-^2 + \frac{2p_-}{c} - 1 \right) = \frac{-2(1 + c^2) w_- p_- \sqrt{Q}}{c(c\sqrt{Q} + ac^2 + 2(mc + a))} < 0,$$

which implies that E_- is a saddle and it is unstable. The proof of (II)(i) is completed.

For the positive equilibrium E_+, we have

$$\mathrm{Det}(J)|_{E_+} = \frac{w_+ p_+ \sqrt{Q}}{2c(mc + a)^2} \left(c\sqrt{Q} + ac^2 + 2(mc + a) \right) > 0. \tag{13}$$

For determining the stability of E_+, we need to further investigate the sign of $\mathrm{Tr}(J)|_{E_+}$. Using (6) and (9), $\mathrm{Tr}(J)|_{E_+}$ can be rewritten as

$$\mathrm{Tr}(J)|_{E_+} = -1 - p_+^2 + w_+ p_+ \left(1 - \frac{2p_+}{c} \right) = -1 - p_+^2 + m - \frac{a}{c} + \frac{1}{c} w_+. \tag{14}$$

First, notice that $1 - 2p_+/c \leqslant 0$ is equivalent to $a \geqslant mc + 4m/c$. This, together with (14), implies that

$$\mathrm{Tr}(J)|_{E_+} < 0 \quad \text{for } a \geqslant mc + \frac{4m}{c}. \tag{15}$$

Based on (9), p_+ can be rewritten as

$$p_+ = \frac{c + \sqrt{c^2 - 4mc(\frac{mc}{a^2} + \frac{1}{a})}}{2(\frac{mc}{a} + 1)}, \tag{16}$$

which obviously implies that p_+ monotonically increases with respect to a, and p_+ monotonically decreases with respect to m. Thus, we have

$$\frac{\partial p_+}{\partial a} > 0, \qquad \frac{\partial p_+}{\partial m} < 0, \tag{17}$$

which, together with $w_+ = a/(1+p_+^2)$, implies that w_+ monotonically increases with respect to m, i.e., $\partial w_+/\partial m > 0$.

From (6) and (16) and noticing that

$$1 - \frac{p_+}{c} = \frac{mc}{(mc+a)} + \frac{p_-}{c} > 0, \tag{18}$$

we also have

$$w_+ = \frac{m}{p_+(1-\frac{p_+}{c})}. \tag{19}$$

Using (19), it is easy to see that w_+ is decreasing with the increasing of p_+ for $0 < p_+ < c/2$, and w_+ is increasing with the increasing of p_+ for $c/2 < p_+ < c$. In addition, notice that $a < mc + 4m/c$ is equivalent to $p_+ < c/2$. This, together with (17), implies that

$$\frac{\partial w_+}{\partial a} < 0 \quad \text{for } a_* < a < mc + \frac{4m}{c}. \tag{20}$$

For fixed $c > 0$, set

$$F(m,a) \triangleq \operatorname{Tr}(J)|_{E_+} = -1 - p_+^2 + m - \frac{a}{c} + \frac{1}{c}w_+. \tag{21}$$

Then $F(m,a) = 0$ is equivalent to $\operatorname{Tr}(J)|_{E_+} = 0$. It follows from (17) and (20) that for $a_* < a < mc + 4m/c$,

$$\frac{\partial F}{\partial a} = -2p_+\frac{\partial p_+}{\partial a} - \frac{1}{c} + \frac{1}{c}\frac{\partial w_+}{\partial a} < 0, \tag{22}$$

and

$$\frac{\partial F}{\partial m} = -2p_+\frac{dp_+}{dm} + 1 + \frac{1}{c}\frac{dw_+}{dm} > 0. \tag{23}$$

For fixed $m \in (0,\, 2 + 2/c^2]$, it follows from (25) that

$$\lim_{a \to a_*^+} \operatorname{Tr}(J)\big|_{E_+} = \operatorname{Tr}(J)|_{E_*} \leqslant 0,$$

which, together with (15) and (22), implies that for $a_* < a < mc + 4m/c$,

$$\operatorname{Tr}(J)|_{E_+} < \lim_{a \to a_*^+} \operatorname{Tr}(J)|_{E_+} < 0.$$

This implies that $E_+(w_+, p_+)$ is locally asymptotically stable for $m \in (0,\, 2 + 2/c^2]$.

Then we consider the case of $m > 2 + 2/c^2$. From (8) and (14) we have

$$\lim_{a \to a_*^+} \operatorname{Tr}(J)\big|_{E_+} = \operatorname{Tr}(J)|_{E_*} > 0 \quad \text{for } m > 2 + \frac{2}{c^2}. \tag{24}$$

Continuous function intermediate value theorem, together with (15) and (24), implies that for fixed c and $m > 2 + 2/c^2$, there exists a function $a = a_H(m)$ with

$$a_* < a_H(m) < mc + \frac{4m}{c}$$

such that $\mathrm{Tr}(J)|_{E_+} = 0$ at $a = a_H(m)$. This, together with (13), implies that the characteristic equation (12) has a pair of purely imaginary roots $\pm\sqrt{\mathrm{Det}(J)|_{E_+}}$ at $a = a_H(m)$ for $m > 2 + 2/c^2$. Taking a as a parameter and letting $\lambda = \lambda(a)$ be a root of Eq. (12) satisfying $\lambda(a_H(m)) = \sqrt{\mathrm{Det}(J)|_{E_+}}$, we obtain the following transversality condition from (12), (21), and (22):

$$\mathrm{Re}\left(\frac{\mathrm{d}\lambda}{\mathrm{d}a}\right)\Big|_{a=a_H(m)} = \frac{1}{2}\frac{\partial\,\mathrm{Tr}(J)|_{E_+}}{\partial a}\Big|_{a=a_H(m)} = \frac{1}{2}\frac{\partial F}{\partial a}|_{a=a_H(m)} < 0.$$

This implies that system (5) undergoes a Hopf bifurcation at $a = a_H(m)$.

Furthermore, for fixed $c > 0$, $\mathrm{Tr}(J)|_{E_+} = 0$ can determine an implicit function near $(m, a_H(m))$. In the following, we investigate the monotonicity of $a = a_H(m)$ as a function of m. The monotonicity of the function $a = a_H(m)$ with respect to m can be easily shown as follows. It follows from (22) and (23) that

$$\frac{da_H(m)}{dm} = -\frac{\partial F/\partial m}{\partial F/\partial a} > 0.$$

Then the proof of conclusion (II)(ii) is completed.

When $a = a_*$, it follows from Theorem 1 that system (5) has only one positive equilibrium $E_*(w_*, p_*)$. Letting $s = \sqrt{1+c^2}$, by (6), (7), and (8), a_*, w_* and p_* can be rewritten as

$$a_* = \frac{2m(s+1)}{c}, \qquad p_* = \frac{c}{s+1}, \qquad w_* = \frac{m(s+1)^2}{cs}.$$

For simplification of notation, from (11), denoting the characteristic matrix J_{E_*} by A, we have

$$A = \begin{pmatrix} -\frac{2s}{s+1} & -\frac{2m(s+1)}{s} \\ \frac{s(s-1)}{(s+1)^2} & \frac{m(s-1)}{s} \end{pmatrix},$$

and then

$$\mathrm{Det}(A) = 0, \qquad \mathrm{Tr}(A) \begin{cases} < 0, & m < 2 + \frac{2}{c^2}, \\ = 0, & m = 2 + \frac{2}{c^2}, \\ > 0, & m > 2 + \frac{2}{c^2}, \end{cases} \tag{25}$$

which implies that Eq. (12) has a zero root and a negative root for $a = a_*$ and $m < 2 + 2/c^2$, a zero root and a positive root for $a = a_*$ and $m > 2 + 2/c^2$.

For the case of $a = a_*$ and $m \neq 2 + 2/c^2$, the left eigenvector ξ and right eigenvector η of A for the zero eigenvalue can be chosen as

$$\xi = \begin{pmatrix} \frac{m(s+1)^2}{s^2} \\ -1 \end{pmatrix}, \qquad \eta = \begin{pmatrix} \frac{s-1}{s+1} \\ 2 \end{pmatrix}.$$

Denoting the vector field of system (5) by

$$f(w, p, a) = \begin{pmatrix} a - w - wp^2 \\ wp^2(1 - \frac{p}{c}) - mp \end{pmatrix},$$

we can verify the following nondegeneracy conditions:

$$\eta^{\top} f'_a(w_*, p_*, a_*) = \frac{\sqrt{1+c^2}-1}{\sqrt{1+c^2}+1} > 0,$$
$$\eta^{\top} D^2_{(w,p)} f(w_*, p_*, a_*)(\xi, \xi) = -\frac{2m(1+\sqrt{1+c^2})^2}{c\sqrt{1+c^2}} < 0.$$

According to the results in [9], when $m \neq 2 + 2/c^2$, system (5) undergoes a saddle-node bifurcation at $a = a_*$. From (25) and noticing that $\mathrm{Det}(A) = 0$, it is easy to verify that the characteristic equation (12) has double zero roots for $a = a_*$ and $m = 2+2/c^2$. Then conclusion (II)(iii) is confirmed. □

3 Stability and diffusion-driven Turing instability for the system without nonlocal terms

In this section, we consider system (4) under the case of local infiltration and local absorption, i.e., the following reaction–diffusion system:

$$\begin{aligned} \frac{\partial w}{\partial t} &= dw_{xx} + a - w - wp^2, \\ \frac{\partial p}{\partial t} &= p_{xx} + wp^2\left(1 - \frac{p}{c}\right) - mp. \end{aligned} \tag{26}$$

Notice that the equilibrium of ODE system (5) is still the constant steady state of (26).

In what follows, we will analyze the influence of diffusion on the stability of the positive constant steady state $E_+ = (w_+, p_+)$ under the assumption that it is locally asymptotically stable when E_+ is considered as the corresponding ODE system (5). Therefore, in this section, we always assume that the following condition holds:

(C$_0$) $\mathrm{Tr}(J)|_{E_+} < 0, \mathrm{Det}(J)|_{E_+} > 0.$

Assume that the solution of the linearized system of (26) at $E_+ = (w_+, p_+)$ is of the form

$$\begin{pmatrix} w \\ p \end{pmatrix} = \begin{pmatrix} a_k \\ b_k \end{pmatrix} \mathrm{e}^{\lambda t + \mathrm{i}kx}, \tag{27}$$

where $a_k, b_k, k \in \mathbb{R}$, $\lambda \in \mathbb{C}$, and i denotes the imaginary unit. Then, substituting (27) into the linearized system of (26) at $E_+ = (w_+, p_+)$, we have the following characteristic equation:

$$\lambda^2 - T(k,d)\lambda + D(k,d) = 0, \tag{28}$$

where

$$T(k,d) = -1 - p_+^2 + w_+p_+\left(1 - \frac{2p_+}{c}\right) - k^2(d+1) < 0, \tag{29}$$

$$D(k,d) = dk^4 - \left[d\left(1 - \frac{2p_+}{c}\right)w_+p_+ - \left(1+p_+^2\right)\right]k^2 + \mathrm{Det}(J)|_{E_+}. \tag{30}$$

Via analyzing the distribution of roots of Eq. (28), we have the following results on the stability and diffusion-driven Turing instability on E_+.

Theorem 3. *Assume that $a > 2m(1+\sqrt{1+c^2})/c$. For the positive constant steady state E_+ of system* (26)*, $a_H(m)$ is defined as in Theorem* 2*. Then we have the following results*:

(i) *if $a \geqslant mc + 4m/c$, E_+ is asymptotically stable for any $d > 0$;*

(ii) *if $a_H(m) < a < mc + 4m/c$, then there exists a critical value $d_c > 1$ with*

$$d_c = \frac{p_+^2 + \frac{2p_+}{c} - 1 + 2p_+^2(1-\frac{p_+}{c}) + 2p_+\sqrt{2(p_+^2+\frac{2p_+}{c}-1)(1-\frac{p_+}{c})}}{(1-\frac{2p_+}{c})^2 w_+ p_+} \tag{31}$$

such that E_+ is asymptotically stable for $0 < d < d_c$ and unstable for $d > d_c$, Turing bifurcation occurs at $d = d_c$ with the critical wave number k_c, where

$$k_c = \sqrt{\frac{d_c(1-\frac{2p_+}{c})w_+p_+ - (1+p_+^2)}{2d_c}}. \tag{32}$$

Proof. Noting that $\mathrm{Det}(J)|_{E_+} > 0$ and that $1-2p_+/c \leqslant 0$ if and only if $a \geqslant mc+4m/c$, we conclude that if $a \geqslant mc + 4m/c$, then $D(k,d) > 0$ for any $d > 0$ and $k \in \mathbb{R}$. In addition, it follows from (29) that $T(k,d) < 0$ for any $d > 0$ and $k \in \mathbb{R}$. This implies that all roots of the characteristic equation (28) have negative real parts, which completes the proof of conclusion (i).

If $a < mc + 4m/c$, then $1 - 2p_+/c > 0$. From (30) it is easy to verify that when $0 < d \leqslant d_*$, we still have $D(k,d) > 0$ for any $k \in \mathbb{R}$ because

$$d\left(1-\frac{2p_+}{c}\right)w_+p_+ - \left(1+p_+^2\right) < 0$$

is equivalent to $d \leqslant d_*$, where

$$d_* = \frac{1+p_+^2}{(1-\frac{2p_+}{c})w_+p_+}. \tag{33}$$

When $d > d_*$, the symmetry axis of the function $D(k,d)$ is $k^2 = k_s^2$ with

$$k_s(d) = \sqrt{\frac{d(1-\frac{2p_+}{c})w_+p_+ - (1+p_+^2)}{2d}}.$$

Denote the minimum value of $D(k_s,d)$ by $D_{\min}(d)$. Then we have

$$\begin{aligned} D_{\min}(d) &= D\big(k_s(d),d\big) \\ &= \frac{1}{4}\bigg[-\left(1-\frac{2p_+}{c}\right)^2 w_+^2p_+^2 d - \frac{(1+p_+^2)^2}{d} \\ &\quad + 2\left(-\frac{2p_+^3}{c} + 3p_+^2 + \frac{2p_+}{c} - 1\right)w_+p_+\bigg], \end{aligned} \tag{34}$$

and the derivative of $D_{\min}(d)$ with respect to d is

$$D'_{\min}(d) = \frac{1}{4}\left[-\left(1-\frac{2p_+}{c}\right)^2 w_+^2 p_+^2 + \frac{(1+p_+^2)^2}{d^2}\right] \to \begin{cases} > 0, & 0 < d < d_*, \\ < 0, & d > d_*. \end{cases} \tag{35}$$

In addition, notice that $D_{\min}(d_*) = \mathrm{Det}(J)|_{E_+} > 0$. Then solving $D_{\min}(d) = D(k_s, d) = 0$ for $d > d_* > 0$, we have $d = d_c > d_*$, where d_c is defined by (31). Then from (35) it is easy to see that $D_{\min}(d) = D(k_s(d), d) > 0$ for $d < d_c$ and $D_{\min}(d) = D(k_s(d), d) < 0$ for $d > d_c$. For the critical value $d = d_c$, we denote $k_c = k_s(d_c)$, as defined by (32), for the simplification of notation. Generally, k_c is called the critical wave number. By $\mathrm{Tr}(J)|_{E_+} < 0$, it is easy to see that $d_* > 1$, and then $d_c > d_* > 1$.

The above arguments implies that for $0 < d < d_c$, all roots of the characteristic equation (28) have negative real parts for any $k \in \mathbb{R}$. For $d = d_c$, the characteristic equation (28) has only one zero root for $k = k_c$, and all other roots have negative real parts for $k \neq k_c$. For $d > d_c$, there exist an interval $I_c \subset \mathbb{R}^+$ such that (28) has positive real root for $k^2 \in I_c$. This completes the proof of conclusion (ii). □

For fixed $c > 0$, define three regions in the m, a-plane:

$$I = \left\{(m,a) \;\middle|\; a \geqslant mc + \frac{4m}{c},\ m > 0\right\},$$

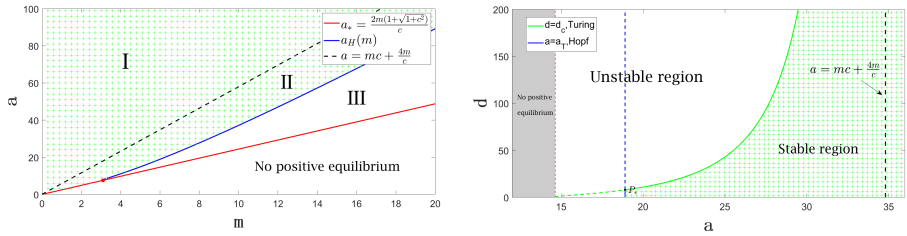
$$II = \left\{(m,a) \;\middle|\; \frac{2m(1+\sqrt{1+c^2})}{c} < a < mc + \frac{4m}{c},\ 0 < m \leqslant 2 + \frac{2}{c^2}\right\} \cup \left\{(m,a) \;\middle|\; a_H(m) < a < mc + \frac{4m}{c},\ m > 2 + \frac{2}{c^2}\right\},$$

$$III = \left\{(m,a) \;\middle|\; \frac{2m(1+\sqrt{1+c^2})}{c} < a < a_H(m),\ m > 2 + \frac{2}{c^2}\right\}.$$

It follows from Theorem 3 that the positive equilibrium E_+ of the ODE (5) is asymptotically stable for $(m,a) \in I \cup II$ and unstable for $(m,a) \in III$. Based on Theorem 2, the positive equilibrium E_+ of the spatial model (26) is asymptotically stable for $(m,a) \in I$ and unstable for $(m,a) \in II \cup III$. The region II is called Turing instability region. For $c = 5$, Fig. 2(a) shows these stable and unstable regions and the bifurcation curves.

For $c = 5$, $m = 6$, we obtain Hopf bifurcation point $a_H \doteq 18.9037$, which is on the Hopf bifurcation curve of Fig. 2. Figure 2(b) illustrates the Turing bifurcation curve and Hopf bifurcation straight line in a, d-plane for $c = 5$, $m = 6$. Turing bifurcation curve and Hopf bifurcation straight line intersect at $P_* = (18.9037, 8.1348)$.

Remark. When $a \to mc + 4m/c$ ($p_+ \to c/2$), we have $d_c \to +\infty$.



(a) (b)

Figure 2. a) The positive equilibrium E_+ of the ODE (5) is asymptotically stable for $(m, a) \in I \cup II$ and unstable for $(m, a) \in III$; (b) stable region and bifurcation diagrams in a, d-plane for system (26) with $m = 6$, $c = 5$. The black dotted line is the vertical asymptotic line of the curve $d = d_c$.

4 Spatiotemporal dynamics induced by the nonlocal effects

In this section, we investigate the spatiotemporal dynamics induced by the nonlocal effects for two kinds of kernel functions: (i) spatial average kernel in the finite domain; (ii) Top-hat kernel in the infinite domain.

4.1 Turing instability for the spatial average kernel

We choose one-dimensional spatial domain $\Omega = [-L, L]$, and the nonlocal effects are characterized by the following forms:

$$K * p = \frac{1}{2L}\int_{-L}^{L} p(y,t)\,\mathrm{d}y, \qquad K * w = \frac{1}{2L}\int_{-L}^{L} w(y,t)\,\mathrm{d}y,$$

which are the average value of p and w on the whole domain $\Omega = [-L, L]$ at time t. In this subsection, we consider the following nonlocal system subject to homogeneous Neumann boundary conditions:

$$\begin{aligned}
&\frac{\partial w}{\partial t} = d\frac{\partial^2 w}{\partial x^2} + a - w - w\left(\frac{1}{2L}\int_{-L}^{L} p(y,t)\,\mathrm{d}y\right)^2, \quad x \in (-L, L),\ t > 0,\\
&\frac{\partial p}{\partial t} = \frac{\partial^2 p}{\partial x^2} + \left(\frac{1}{2L}\int_{-L}^{L} w(y,t)\,\mathrm{d}y\right)p^2\left(1 - \frac{p}{c}\right) - mp, \quad x \in (-L, L),\ t > 0,\\
&\frac{\partial w}{\partial x}(-L,t) = \frac{\partial w}{\partial x}(L,t) = 0, \quad \frac{\partial p}{\partial x}(-L,t) = \frac{\partial p}{\partial x}(L,t) = 0, \quad t \geqslant 0.
\end{aligned} \tag{36}$$

Notice that the corresponding ordinary differential equations of system (36) is system (5), and thus the equilibrium of system (5) is also constant steady state of system (36). In what follows, we investigate the influence of the nonlocal average on E_+ and the possible patterns. We also assume that condition (C_0) holds in this subsection.

The characteristic equation after the linearization at E_+ for system (36) is

$$\Gamma_n(\lambda) = \lambda^2 - T_n\lambda + D_n = 0,\ n \in \mathbb{N}_0,$$

where

$$T_n = -1 - p_+^2 + w_+p_+\left(1 - \frac{2p_+}{c}\right) - \left(\frac{n\pi}{L}\right)^2(d+1), \tag{37}$$

$$\begin{aligned} D_n = {} & d\left(\frac{n\pi}{L}\right)^4 - \left[dw_+p_+\left(1 - \frac{2p_+}{c}\right) - \left(1 + p_+^2\right)\right]\left(\frac{n\pi}{L}\right)^2 \\ & - w_+p_+\left(1 + p_+^2\right)\left(1 - \frac{2p_+}{c}\right) + 2w_+p_+^3\left(1 - \frac{p_+}{c}\right)\chi_n^2. \end{aligned} \tag{38}$$

Here $\chi_0 = 1$ and $\chi_n = 0$ for $n \in \mathbb{N}$.

Notice that $T_0 = \mathrm{Tr}(J)|_{E_+}$, $D_0 = \mathrm{Det}(J)|_{E_+}$. Therefore, under condition (C_0), it is easy to see from (37) that $T_n < 0$ for any $n \in \mathbb{N}_0$ and $D_0 > 0$. For $n \in \mathbb{N}$, we have $\chi_n^2 = 0$, and (38) becomes

$$\begin{aligned} D_n = {} & d\left(\frac{n\pi}{L}\right)^4 - \left[dw_+p_+\left(1 - \frac{2p_+}{c}\right) - \left(1 + p_+^2\right)\right]\left(\frac{n\pi}{L}\right)^2 \\ & - w_+p_+\left(1 + p_+^2\right)\left(1 - \frac{2p_+}{c}\right). \end{aligned} \tag{39}$$

It is easy to obtain that when $(m, a) \in I$ (i.e., $1 - 2p_+/c \leqslant 0$), $D_n > 0$ always holds for any $n \in \mathbb{N}_0$. Then we consider the case of $(m, a) \in II$ (i.e., $1 - 2p_+/c > 0$). In this case, we have

$$-w_+p_+(1 + p_+^2)(1 - \frac{2p_+}{c}) < 0.$$

Therefore, for any $n \in \mathbb{N}$, we can choose the appropriate domain size L such that $D_n < 0$. For fixed d, we can consider (39) as a quadratic function of $(n\pi/L)^2$. By simple calculation, we can obtain that for any $n \in \mathbb{N}$, there exists a critical value $L_c(n)$ of L such that $D_n > 0$ for $L < L_c(n)$ and $D_n \leqslant 0$ for $L \geqslant L_c(n)$, where

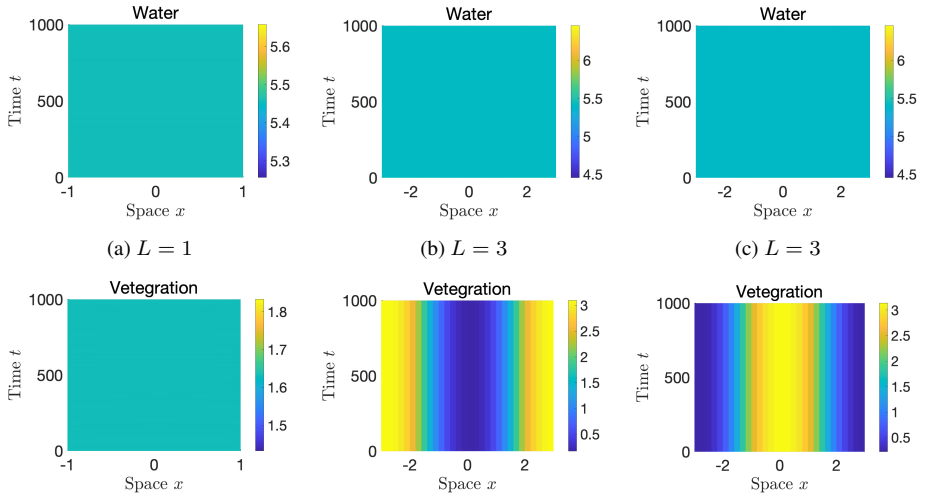
$$L_c(n) = \frac{n\pi}{\sqrt{w_+p_+(1 - \frac{2p_+}{c})}}. \tag{40}$$

Since (40) is monotonically increasing with respect to n, we can define

$$L_c \triangleq L_c(1) = \frac{\pi}{\sqrt{w_+p_+(1 - \frac{2p_+}{c})}}. \tag{41}$$

When $L < L_c$, we have $D_n > 0$ for any $n \in \mathbb{N}$, when $L = L_c$, we have $D_1 = 0$ and $D_n > 0$ for $n \in \mathbb{N}$ with $n \neq 1$, and when $L > L_c$, there exists at least one $n \in \mathbb{N}$ such that $D_n < 0$.

By the above discussion, it is easy to obtain the following results on the stability and bifurcaton.



(a) $L = 1$ (b) $L = 3$ (c) $L = 3$

(d) $L = 1$ (e) $L = 3$ (f) $L = 3$

Figure 3. (a) and (d) E_+ is asymptotically stable for $L = 1 < L_c$; (b) and (e) for $L = 3 > L_c$, there exists mode-1 spatially inhomogeneous steady state; (c) and (f) for $L = 3 > L_c$ and the initial functions different from those used in (b) and (e), there exists another mode-1 spatially inhomogeneous steady state.

Theorem 4. *For system* (36)*, considering* L *as the bifurcation parameter, we have the following results*:

(I) *when* $a \geqslant mc + 4m/c$, E_+ *is always asymptotically stable for any* $L > 0$;

(II) *when* $a_H(m) < a < mc + 4m/c$, *there exists a critical value* L_c *such that* E_+ *is stable for* $L < L_c$ *and unstable for* $L > L_c$, *and system* (36) *undergoes mode*-1 *steady state bifurcation at* $L = L_c$.

It has been shown from Theorem 4 that the domain size can drive patterns and that the corresponding critical value is independent of the diffusion coefficient d. For the parameters $a = 20$, $m = 6$, $c = 5$ such that $a_H(m) < a < mc + 4m/c$, it follows from (9) and (41) that

$$(w_+, p_+) \doteq (5.4573, 1.6325), \qquad L_c \doteq 1.7868. \tag{42}$$

For numerical simulation, we choose $d = 5$, and Fig. 3 illustrates the simulation results of model (36) for different spatial lengths. It follows from Theorem 4 that system (36) undergoes mode-1 Turing bifurcation at $L = L_c$. For $L = 1 < L_c \doteq 1.7868$, E_+ is asymptotically stable as shown in Figs. 3(a) and 3(d). When the system undergoes a mode-1 Turing bifurcation, it may correspond to one of three canonical scenarios: a saddle–node bifurcation, a pitchfork bifurcation, or a transcritical bifurcation. While a rigorous identification of the bifurcation type requires the computation of the associated normal form, such a formal proof lies beyond the scope of the present work. Nevertheless, numerical evidence strongly suggests that the observed instability manifests as a supercritical pitchfork bifurcation. Specifically, as the domain size L varies in the vicinity of

the critical value L_c, we observe the following behavior: for $L < L_c$, no nonconstant steady states exist in the neighborhood of the homogeneous equilibrium; for $L > L_c$, two stable nonconstant steady states emerge (see Figs. 3(e) and 3(f)). Consequently, for $L > L_c$, the long-time asymptotic behavior of the system is initial-condition dependent. Figures 3(e) and 3(f) illustrate two symmetric nonconstant steady states.

4.2 Different patterns induced by the top-hat kernel

For the infinite domain $\Omega = (-\infty, +\infty)$, we consider

$$K * p = \int_{-\infty}^{+\infty} \phi_M(x-y)p(y,t)\,\mathrm{d}y, \qquad K * w = \int_{-\infty}^{+\infty} \phi_M(x-y)w(y,t)\,\mathrm{d}y, \tag{43}$$

where the kernel function is chosen as the so-called Top-hat kernel function

$$\phi_M(x) = \begin{cases} \frac{1}{M}, & |x| \leqslant M, \\ 0, & |x| > M, \end{cases}$$

in which M measures the scale of nonlocality. In this subsection, we investigate the influence of the nonlocal scale on E_+ and the possible patterns.

The linearized system of (4) at $E_+ = (w_+, p_+)$ is

$$\begin{pmatrix} w_t \\ p_t \end{pmatrix} = D \begin{pmatrix} w_{xx} \\ p_{xx} \end{pmatrix} + A_1 \begin{pmatrix} w \\ p \end{pmatrix} + A_2 \begin{pmatrix} K * w \\ K * p \end{pmatrix} \tag{44}$$

with $D = \operatorname{diag}\{d, 1\}$ and

$$A_1 = \begin{pmatrix} -1 - p_+^2 & 0 \\ 0 & w_+p_+(1 - \frac{2p_+}{c}) \end{pmatrix}, \qquad A_2 = \begin{pmatrix} 0 & -2w_+p_+ \\ p_+^2(1 - \frac{p_+}{c}) & 0 \end{pmatrix}.$$

We assume that the solution of (44) is of the form

$$\begin{pmatrix} w \\ p \end{pmatrix} = \begin{pmatrix} a_k \\ b_k \end{pmatrix} \mathrm{e}^{\lambda t + \mathrm{i}kx}, \tag{45}$$

where $\lambda \in \mathbb{C}$, $k \in \mathbb{R}$. For this solution, it is easy to verify that $K * p = pH(k, M)$ and $K * w = wH(k, M)$, where

$$H(k, M) = \frac{1}{2M} \int_{-M}^{+M} \mathrm{e}^{-\mathrm{i}kz}\,\mathrm{d}z = \begin{cases} \frac{\sin(kM)}{kM}, & k \neq 0, \\ 1, & k = 0. \end{cases} \tag{46}$$

Then, substituting (45) into (44), we obtain the characteristic equation

$$\Gamma_k(\lambda) = \lambda^2 - T(k, d)\lambda + \widetilde{D}(k, d, M) = 0, \tag{47}$$

where $T(k,d)$ is defined by (29), and

$$\begin{aligned}\widetilde{D}(k,d,M) = dk^4 - \left[dw_+p_+\left(1-\frac{2p_+}{c}\right) - \left(1+p_+^2\right)\right]k^2 \\ - w_+p_+\left(1+p_+^2\right)\left(1-\frac{2p_+}{c}\right) \\ + 2w_+p_+^3\left(1-\frac{p_+}{c}\right)H^2(k,M).\end{aligned} \tag{48}$$

Notice that $\lim_{M\to 0^+} H(k,M) = 1$. By (30) and (48), we have $\lim_{M\to 0^+} \widetilde{D}(k,d,M) = D(k,d)$, and by (46) and (48), we have $\widetilde{D}(0,d,M) = D(0,d) > 0$, provided that condition (C_0) holds. In what follows, for $M > 0$, we first investigate the distribution of roots of Eq. (47) under condition (C_0). Obviously, we have $T(k) < 0$ for any $k \in \mathbb{R}$ when condition (C_0) is satisfied.

From (18) we have $1 - p_+/c > 0$, then it follows from (48) that $\widetilde{D}(k,d,M) > 0$ if and only if

$$H^2(k,M) > G(k,d), \tag{49}$$

where

$$G(k,d) = G_1(d)k^4 + G_2(d)k^2 + G_3 \tag{50}$$

with

$$\begin{aligned}&G_1(d) = -\frac{d}{2w_+p_+^3(1-\frac{p_+}{c})}, \qquad G_3 = \frac{(1+p_+^2)(1-\frac{2p_+}{c})}{2p_+^2(1-\frac{p_+}{c})}, \\ &G_2(d) = \frac{dw_+p_+(1-\frac{2p_+}{c}) - (1+p_+^2)}{2w_+p_+^3(1-\frac{p_+}{c})}.\end{aligned} \tag{51}$$

For further analysis, we first introduce the following proposition, which is useful for studying inequality (49).

Proposition 1. *Letting $h(z) = \sin^2 z/z^2$ and denoting the countably infinite number of positive roots of the equation $\tan z = z$ by $z_j > 0$ with $0 < z_j < z_{j+1}$, $j \in \mathbb{N}$, we have the following properties on $h(z)$:*

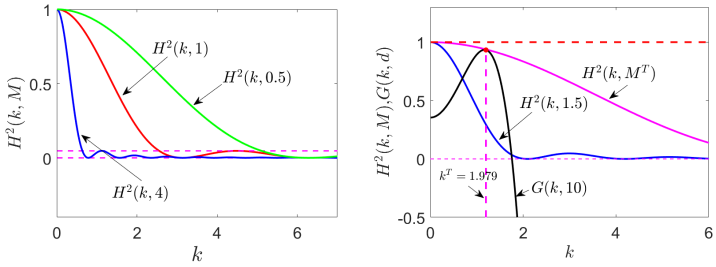
(I) *$h(z)$ obtains its local maximum at $z = z_j$, and*

$$h(z_j) > h(z_{j+1}) > 0, \quad z_j \in \left(j\pi,\, j\pi + \frac{\pi}{2}\right);$$

(II) *$h(z)$ obtains its local minimum at $z = j\pi$, and $h(j\pi) = 0$.*

Proof. By a simple calculation, we have $\lim_{z\to 0} h(z) = 1$ and

$$\frac{d\,h(z)}{d\,z} = \frac{2\sin z(z\cos z - \sin z)}{z^3}.$$



(a) (b)

Figure 4. (a) The graphs of the function $h = h(kM)$ for $M = 4$, $M = 1$, $M = 0.5$. (b) For $0 < d < d_c$, there exists M^T such that $G(k,d)$ and $h(kM^T)$ are tangent at $k = k^T$. Here $a = 20$, $m = 6$, $c = 5$, and $d = 10$.

Because z_j is the positive roots of the equation $\tan z = z$ with $0 < z_j < z_{j+1}$, it is easy to see that

$$z_j \in \left(j\pi,\, j\pi + \frac{\pi}{2}\right) \quad \text{and} \quad z_j - j\pi < z_{j+1} - (j+1)\pi, \quad j \in \mathbb{N}, \tag{52}$$

and

$$\frac{\mathrm{d}h(z)}{\mathrm{d}z} \begin{cases} > 0, & z \in (j\pi, z_j), \\ < 0, & z \in (z_j,\, (j+1)\pi), \\ 0, & z = z_j. \end{cases}$$

From $z_j = \tan z_j$ we have

$$h(z_j) = \frac{\sin^2 z_j}{z_j^2} = \cos^2 z_j. \tag{53}$$

Then from (52) and (53) we can conclude that $h(z_j) > h(z_{j+1}) > 0$. This completes the proof of the proposition. □

Figure 4(a) illustrates the graph of the function $h = h(kM) = H^2(k,M)$ for different values of M and intuitively shows the results of Proposition 1.

Again, noting that $1 - p_+/c > 0$, we conclude that $1 - 2p_+/c \leqslant 0$ is equivalent to $a \geqslant mc + 4m/c$. From (50) and (51) it follows that $G(d,k) < 0$ for any $d > 0$ and $k \neq 0$, which, together with $H^2(k,M) \geqslant 0$, implies that inequality (49) holds for $d > 0$ and $k \neq 0$. Therefore if $a \geqslant mc + 4m/c$, then $\widetilde{D}(k,d,M) > 0$ for any $d > 0$ and $k \in \mathbb{R}$. This implies that all roots of the characteristic equation (47) have negative real parts for any $d > 0$ and $k \in \mathbb{R}$, provided that $a \geqslant mc + 4m/c$. Then we have the following results.

Theorem 5. *For system* (4) *with the nonlocal terms* (43)*, if $a \geqslant mc + 4m/c$, then the positive steady state E_+ is always asymptotically stable for any $d > 0$ and $M > 0$.*

In the following, we consider the case of $a_H(m) < a < mc + 4m/c$. For this case, we first have the following results on the distribution of roots of Eq. (47)

Lemma 1. *Assume that $a_H(m) < a < mc + 4m/c$ and d_c is defined by* (31).

(I) *If $0 < d < d_c$, then there exist critical values M^T and k^T satisfying*

$$H^2\big(k^T, M^T\big) = G\big(k^T, d\big), \qquad \frac{\partial}{\partial k} H^2\big(k^T, M^T\big) = \frac{\partial}{\partial k} G\big(k^T, d\big)$$

such that

(i) *for $M \in (0, M^T)$, $\widetilde{D}(k, d, M) > 0$ for $k \in \mathbb{R}$;*

(ii) *for $M = M^T$, $\widetilde{D}(k^T, d, M^T) = 0$ and $\widetilde{D}(k, d, M^T) > 0$ for $k \neq k^T$;*

(iii) *for $M \in (M^T, +\infty)$, there exists at least one $k > 0$ satisfying the inequality $\widetilde{D}(k, d, M) < 0$.*

(II) *If $d \geqslant d_c$, for any $M > 0$, there exists at least one $k > 0$ such that the inequality $\widetilde{D}(k, d, M) < 0$ holds.*

Proof. Since $\widetilde{D}(k, d, M)$ is an even function with respect to k, it is enough only to consider the case of $k > 0$. According to (48), we have that $\widetilde{D}(k, d, M) > 0$ is equivalent to $H^2(k, M) > G(k, d)$. Thus, we need to compare the $\max_{k>0}\{G(k, d)\}$ with $\sup_{k>0}\{H^2(k, M)\} = 1$.

Taking the partial derivative of $G(k, d)$ with respect to k, we obtain

$$\frac{\partial G(k, d)}{\partial k} = \frac{k\{4dk^2 - 2[dw_+p_+(1 - \frac{2p_+}{c}) - (1 + p_+^2)]\}}{-2w_+p_+^3(1 - \frac{p_+}{c})}. \tag{54}$$

When $d > d_*$, where d_* is defined by (33), we have $d(1 - 2p_+/c)w_+p_+ - (1 + p_+^2) > 0$, while for $d \leqslant d_*$, $d(1 - 2p_+/c)w_+p_+ - (1 + p_+^2) \leqslant 0$.

Then, for $d > d_*$, we have

$$\frac{\partial G(k, d)}{\partial k} \begin{cases} > 0, & 0 < k < k_*, \\ < 0, & k > k_*, \end{cases}$$

where

$$k_* = \sqrt{\frac{dw_+p_+(1 - \frac{2p_+}{c}) - (1 + p_+^2)}{2d}},$$

which indicates that for fixed $d \in (d_*, +\infty)$, $G(k, d)$ is increasing for $k \in (0, k_*)$ and decreasing for $k \in (k_*, +\infty)$, and we can obtain

$$\max_{k>0}\big\{G(k, d)\big\} = G(k_*, d) = \frac{[dw_+p_+(1 - \frac{2p_+}{c}) + (1 + p_+^2)]^2}{8dw_+p_+^3(1 - \frac{p_+}{c})}.$$

By simple calculation, we obtain

$$\begin{aligned} &\max_{k>0}\big\{G(k, d)\big\} - \sup_{k>0}\big\{H^2(k, M)\big\} \\ &\quad = G(k_*, d) - 1 = \frac{-D_{\min}(d)}{2dw_+p_+^3(1 - \frac{p_+}{c})} \begin{cases} < 0, & d_* < d < d_c, \\ \geqslant 0, & d \geqslant d_c, \end{cases} \end{aligned} \tag{55}$$

due to $1-p_+/c>0$ from (18), where $D_{\min}(d)$ is defined by (34). Thus, for $d\in(d_*,d_c)$, we have $\max_{k>0}\{G(k,d)\}<\sup_{k>0}\{H^2(k,M)\}$, and for $d\in[d_c,+\infty)$, we have $\max_{k>0}\{G(k,d)\}\geqslant\sup_{k>0}\{H^2(k,M)\}$.

Similarly, for $0<d\leqslant d_*$,

$$2\left[dw_+p_+\left(1-\frac{2p_+}{c}\right)-\left(1+p_+^2\right)\right]\leqslant 0.$$

According to (54), we have $\partial G(k,d)/\partial k<0$ for any $k>0$, which implies that $G(k,d)$ is monotonically decreasing. Then we have

$$\max_{k\geqslant 0}\big\{G(k,d)\big\}=G(0,d)=G_3=\frac{(1+p_+^2)(1-\frac{2p_+}{c})}{2p_+^2(1-\frac{p_+}{c})}.$$

By simple calculation, we obtain

$$\max_{k>0}\big\{G(k,d)\big\}-\sup_{k>0}\big\{H^2(k,M)\big\}=G_3-1=-\frac{\mathrm{Det}(J)}{2p_+^2(1-\frac{p_+}{c})}<0,$$

which indicates $\max_{k>0}\{G(k,d)\}<\sup_{k>0}\{H^2(k,M)\}$ for $d\in(0,d_*]$.

Based on the above analysis, we have that $\max_{k>0}\{G(k,d)\}<\sup_{k>0}\{H^2(k,M)\}$ must hold for any $d\in(0,d_c)$. We know the fact that $H^2(k,M)$ is an oscillating function of M and k. When M is increasing, the curve $H^2(k,M)$ compresses from right to left along the k-axis, and the local maximums of the function $H^2(k,M)$ keep unchanged, as shown in Fig.4(a). In addition, for fixed M,

$$\lim_{k\to+\infty}H^2(k,M)=0,\qquad\lim_{k\to+\infty}G(k,d)=-\infty.$$

When M is small enough, we can obtain $H^2(k,M)>G(k,d)$ for any $k>0$. When M varies from small to large to $M=M^T$, the curve $H^2(k,M)$ is tangent to the curve $G(k,d)$ at $k=k^T$, as shown in Fig.4(b). Then, for $k\neq k^T$, $H^2(k,M)>G(k,d)$. The proof of conclusion (I)(ii) is completed. For $M\in(0,M^T)$, the curve of $H^2(k,M)$ is to the right of the curve of $H^2(k,M^T)$ on the k-axis. Thus, for any $k>0$, $H^2(k,M)>G(k,d)$. The proof of conclusion (I)(i) is completed. With the increase of M, the curve of $H^2(k,M)$ is compressed along the k-axis. For $M\in(M^T,+\infty)$, $H^2(k,M)$ must cross the curve $G(k,d)$. Thus, there exists at least one $k>0$ such that $H^2(k,M)<G(k,d)$, then $\widetilde{D}(k,d,M)<0$. The proof of conclusion (I)(iii) is completed.

For $d\in[d_c,+\infty)$, we have obtained $\max_{k>0}\{G(k,d)\}\geqslant\sup_{k>0}\{H^2(k,M)\}$ from (55), and the maximum values of $G(k,d)$ and $H^2(k,M)$ are respectively obtained at different k. Thus, for any M, $H^2(k,M)$ must cross the curve $G(k,d)$, which implies that there exists at least one $k>0$ such that $H^2(k,M)<G(k,d)$. The proof of conclusion (II) is completed. □

It follows from Theorem 2 that when $a_H(m)<a<mc+4m/c$ and $0<d<d_c$, E_+ is asymptotically stable and that there is no diffusion-driven Turing instability for the

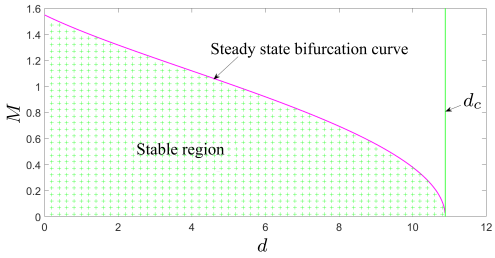


Figure 5. Stability region and bifurcation diagrams in the d,M-plane for system (4) with the nonlocal terms (43) for $a = 20$, $m = 6$, and $c = 5$.

case without nonlocal terms. However, for system (4) with the nonlocal terms (43), the nonlocal scale M can affect the stability of E_+, as shown in the following theorem. In the remainder of this subsection, we focus on this case of $a_H(m) < a < mc + 4m/c$ and $0 < d < d_c$. From Lemma 1 we immediately have the following results on how M affects the stability of E_+.

Theorem 6. *For system* (4) *with the nonlocal terms* (43)*, assume that* $a_H(m) < a < mc + 4m/c$ *and* $0 < d < d_c$*, where* d_c *is defined by* (31)*. Then there exists the critical values* M^T *and* k^T *such that* $H^2(k, M^T)$ *and* $G(k, d)$ *are tangent at* $k = k^T$*.*

(I) E_+ *is always asymptotically stable for* $M \in (0, M^T)$ *and unstable for* $M \in (M^T, +\infty)$;

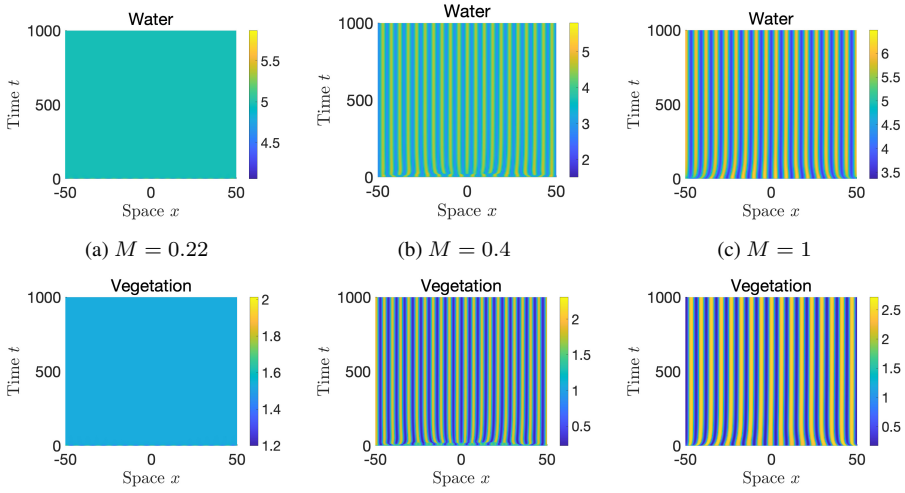
(II) *system* (4) *with the nonlocal terms* (43) *undergoes a steady state bifurcation at* $M = M^T$.

According to the results of Theorem 6, choosing $a = 20$, $m = 6$, $c = 5$, the stability region and bifurcation diagrams in d,M-plane for system (4) with the nonlocal terms (43) is shown in Fig. 5.

For numerical simulations and comparing the results with the case of nonlocal spatial average kernel in Section 4.1, we choose the spatial domain $\Omega = (-L, L)$ and consider system (4) with the nonlocal terms (43) subject to the periodic boundary condition.

Notice that for the periodic boundary condition, the corresponding characteristic equation can be obtained by replacing k with $n\pi/L$ in (47).

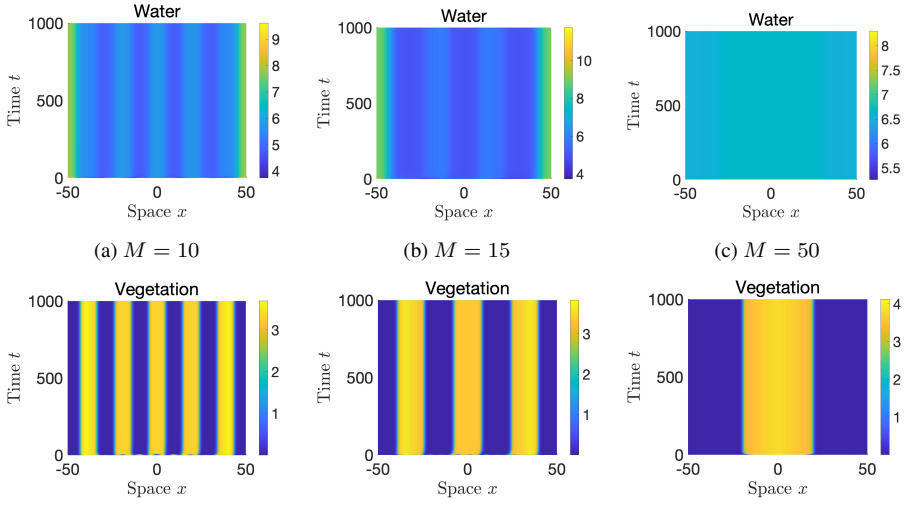
Then we perform numerical simulations to verify the results of the previous analysis. The parameters satisfy $a_H(m) < a < mc + 4m/c$. It follows from (42) and (31) that $d_c \doteq 10.8844$ and $M_T \doteq 0.379$. For fixed spatial domain $L = 50$ and $d = 10 < d_c$, the positive steady state E_+ is asymptotically stable for $M \in [0, M^T)$, as shown in Figs. 6(a) and 6(d) for $M = 0.22 < M^T$. When M increases across the critical value M_T, the nonlocal effects can trigger the spatial patterns, as shown in Figs. 6(b) and 6(e) for $M = 0.4$ and in Figs. 6(c) and 6(f) for $M = 1$. When spatial nonlocality is further enhanced, the distribution of vegetation becomes more concentrated, as shown in Fig. 7. Especially, when $M = L$, the vegetation is clustered in one spatial position, as shown in Figs. 7(c) and 7(f). It has been shown from Fig. 7 that the larger M is, the more concentrated the aggregation of vegetation distribution will be.



(a) $M = 0.22$ (b) $M = 0.4$ (c) $M = 1$

(d) $M = 0.22$ (e) $M = 0.4$ (f) $M = 1$

Figure 6. (a) and (d) E_+ is stable for $M = 0.22 < M^T$; (b) and (e) E_+ is unstable for $M = 0.4 > M^T$; (c) and (f) E_+ is unstable for $M = 1 > M^T$.



(a) $M = 10$ (b) $M = 15$ (c) $M = 50$

(d) $M = 10$ (e) $M = 15$ (f) $M = 50$

Figure 7. Spatial patterns for system (4) with nonlocal terms (43) for M far from the critical value M^T.

5 Conclusion and discussion

In this paper, we propose a novel semiarid water-vegetation model involving both nonlocal infiltration and nonlocal absorption interactions and focus on the influence of the

nonlocal effect on the stability of the positive steady state and the possible spatiotemporal dynamics. The nonlocality is characterized by a so-called top-hat kernel function with the spatial scale M, which measures the scope of influence of nonlocal infiltration and absorption.

We first study the existence and stability of the nonnegative equilibria of the local model. The desert state E_w always exists and is stable. When the rainfall (a) is larger than some critical value, the model possesses two vegetation states: E_- (less vegetation) and E_+ (more vegetation). The less vegetation state is always unstable and the stability of the more vegetation state depends on the rainfall. When the rainfall is small, the vegetation state is unstable. However, when the rainfall continues to increase beyond a certain critical value, the more vegetation state becomes unstable.

For the spatial model without nonlocal infiltration and nonlocal absorption, diffusion-driven Turing instability is investigated for the more vegetation state. The critical value of Turing bifurcation is theoretically determined. The spatial patterns driven by the Turing bifurcation and the oscillatory patterns driven by the interaction of Turing bifurcation and spatially homogeneous Hopf bifurcation are numerically investigated.

The influence of the spatial average kernel and the top-hat kernel on the spatial distribution of the vegetation are both investigated. For the spatial average kernel, only mode-1 spatially inhomogeneous steady state exists. Vegetation gathers in the middle position or near the boundary domain. For the more reasonable top-hat kernel, the scale M of the infiltration affects the spatial distribution of vegetation. When the scale is small enough, the more vegetation state is stable. When the scale is larger than some critical value, the more vegetation state becomes unstable, and there exists spatially inhomogeneous distribution of the vegetation. The spatial distribution of vegetation is influenced by the scale of infiltration. The larger the scale of the infiltration is, the more concentrated the vegetation distribution is.

Author contributions. All authors (Y.L., Y.S., and S.X.) have contributed as follows: methodology, formal analysis, validation, writing – original draft preparation, and software, Y. Lin and S. Xue; writing – review & editing, Y. Song. All authors have read and approved the published version of the manuscript.

Conflicts of interest. The authors declare no conflicts of interest.

Acknowledgment. Authors are very grateful to anonymous reviewer for their valuable comments which greatly improve the original manuscript.

References

1. R. Bastiaansen, P. Carter, A. Doelman, Stable planar vegetation stripe patterns on sloped terrain in dryland ecosystems, *Nonlinearity*, **32**(8):2759–2814, 2019, https://doi.org/10.1088/1361-6544/ab1767.

2. P. D'Odorico, A. Bhattachan, K. F. Davis, S. Ravi, C. W. Runyan, Global desertification: Drivers and feedbacks, *Adv. Water Resour.*, **51**:326–344, 2013, https://doi.org/10.1016/j.advwatres.2012.01.013.
3. W. F. Fagan, E. Gurarie, S. Bewick, A. Howard, R. S. Cantrell, C. Cosner, Perceptual ranges, information gathering, and foraging success in dynamic landscapes, *Am. Nat.*, **189**(5):474–489, 2017, https://doi.org/10.1086/691099.
4. V. Giunta, T. Hillen, M. Lewis, J. R. Potts, Local and global existence for nonlocal multispecies advection-diffusion models, *SIAM J. Appl. Dyn. Syst.*, **21**(3):1686–1708, 2022, https://doi.org/10.1137/21M1425992.
5. G. Guo, Q. Qin, D. Pang, Y. Su, Positive steady-state solutions for a vegetation-water model with saturated water absorption, *Commun. Nonlinear Sci. Numer. Simul.*, **131**:107802, 2024, https://doi.org/10.1016/j.cnsns.2023.107802.
6. C.A. Klausmeier, Regular and irregular patterns in semiarid vegetation, *Science*, **284**(5421): 1826–1828, 1999, https://doi.org/10.1155/2020/2498073.
7. F.T. Maestre, et al., Plant species richness and ecosystem multifunctionality in global drylands, *Science*, **335**(6065):214–218, 2012, https://doi.org/10.1126/science.1215442.
8. S.M. Merchant, W. Nagata, Instabilities and spatiotemporal patterns behind predator invasions with nonlocal prey competition, *Theor. Popul. Biol.*, **80**(4):289–297, 2011, https://doi.org/10.1016/j.tpb.2011.10.001.
9. L. Perko, *Differential Equations and Dynamical Systems*, Volume 7, Springer, New York, 3 edition, 2001, https://doi.org/10.1007/978-1-4613-0003-8.
10. J.F. Reynolds, et al., Global desertification: Building a science for dryland development, *Science*, **316**(5826):847–851, 2007, https://doi.org/10.1126/science.1131634.
11. M. Rietkerk, J. van de Koppel, Regular pattern formation in real ecosystems, *Trends Ecol. Evol.*, **23**(3):169–175, 2008, https://doi.org/10.1016/j.tree.2007.10.013.
12. H.J. Schenk, Root competition: Beyond resource depletion, *J. Ecol.*, **94**(4):725–739, 2006, https://doi.org/10.1111/j.1365-2745.2006.01124.x.
13. J.A. Sherratt, Pattern solutions of the Klausmeier model for banded vegetation in semiarid environments V: The transition from patterns to desert, *SIAM J. Appl. Math.*, **73**(4):1347–1367, 2013, https://doi.org/10.1137/120899510.
14. G.-Q. Sun, H.-T. Zhang, Y.-L. Song, L. Li, Z. Jin, Dynamic analysis of a plant-water model with spatial diffusion, *J. Differ. Equations*, **329**:395–430, 2022, https://doi.org/10.1016/j.jde.2022.05.009.
15. J. von Hardenberg, E. Meron, M. Shachak, Y. Zarmi, Diversity of vegetation patterns and desertification, *Phys. Rev. Lett.*, **87**(19):198101, 2001, https://doi.org/10.1103/PhysRevLett.87.198101.
16. H. Wang, Y. Salmaniw, Open problems in PDE models for knowledge-based animal movement via nonlocal perception and cognitive mapping, *J. Math. Biol.*, **86**(5):71, 2023, https://doi.org/10.1007/s00285-023-01905-9.
17. S. Xue, Y. Song, Spatially nonhomogeneous Hopf and Turing bifurcations driven by the nonlocal effect with the spatial average kernel, *Math. Meth. Appl. Sci.*, **48**(6):6953–6972, 2025, https://doi.org/10.1002/mma.10730.

18. S. Xue, Y. Song, H. Wang, Spatio-temporal dynamics in a reaction-diffusion equation with nonlocal spatial memory, *SIAM J. Appl. Dyn. Syst.*, **23**(1):641–667, 2024, https://doi.org/10.1137/22M1543860.

19. Y.R. Zelnik, S. Kinast, H. Yizhaq, G. Bel, E. Meron, Regime shifts in models of dryland vegetation, *Philos. Trans. R. Soc. Lond., Ser. A, Math. Phys. Eng. Sci.*, **371**(2004):20120358, 2013, https://doi.org/10.1098/rsta.2012.0358.

20. Y.R. Zelnik, E. Meron, G. Bel, Gradual regime shifts in fairy circles, *Proc. Natl. Acad. Sci. USA*, **112**(40):12327–12331, 2015, https://doi.org/10.1073/pnas.1504289112.